Supplementary Information

Wide-field imaging of active site distribution on semiconducting transition metal dichalcogenide nanosheets in electrocatalytic and photoelectrocatalytic processes

Lisi Wen[1], Houkai Chen[1], Rui Hao[1*]

[1]*Department of Chemistry, Southern University of Science and Technology, 518055 Shenzhen China*

Research Center for Chemical Biology and Omics Analysis, Southern University of Science and Technology, 518055 Shenzhen China

Shenzhen Key Laboratory of Functional Proteomics, Southern University of Science and Technology, 518055 Shenzhen, China

Email: haor@sustech.edu.cn

Contents

Supplementary material and methods

Chemicals and materials

Tetraamminecopper (II) sulfate hydrate ($[Cu(NH_3)_4]SO_4 \bullet xH_2O$, 95%), Chlorauric acid ($HAuCl_4$, Au 23.5~23.8%), isopropanol ($(CH_3)_2CHOH$, 99.7%), ethanol (C_2H_5OH, 99.7%), trimethoxy-(1H,1H,2H,2H-heptadecafluorodecyl)silane ($C_{13}H_{13}F_{17}O_3Si$, 98%) were purchased from Aladdin (Shanghai, China). Deionized (DI) water were purchased from Shenzhen Chemical Technology (Shenzhen, China). The bulk n-type MoS_2 crystals and bulk p-type WSe_2 crystals were purchased from Six Carbon Technology Supplies (Shenzhen, China). The platinum wire electrode (0.5 mm diameter), platinum nets electrode (15×15 mm), glassy carbon (GC) electrode (2 mm diameter) and Hg/HgO electrode were purchased from Eilian (Tianjin, China). Indium tin oxide (ITO) glasses (15−30 Ω, 20×20 mm) were purchased from SPI Supplies (USA). Polydimethylsiloxane (PDMS) films (thickness 100 μm) were purchased from Bald Advanced Materials (Hangzhou, China).

Electrode preparation

The indium tin oxide (ITO) working electrodes (20×20 mm) were cleaned by ultrasonication in deionized water, isopropanol, and ethanol for 15 min in each solvent and dried with high-purity nitrogen. Next, the cleaned ITO electrodes were placed in the same vacuum dryer with an anhydrous ethanol solution of trimethoxy(1H,1H,2H,2H-heptadecafluorodecyl)silane ($C_{13}H_{13}F_{17}O_3Si$:C_2H_5OH V:V = 5:95) followed by modifying with gas phase for 72 h. The silane coupling agent modified an “insulating layer” on the surface of ITO.

A multilayer MoS_2/WSe_2 nanosheets were mechanically exfoliated from bulk crystal samples by Nitto Tape and transferred onto modified ITO electrodes. Finally, PDMS membrane with a pore 2

mm in diameter and 100 μm in thickness was transferred onto the prepared ITO electrodes to hold the electrolyte (Fig. S1).

Electrode characterization

Helium ion microscopy (HIM, ORION NanoFab, Zeiss) was used to characterize the morphology of different nanosheets. Atomic force microscopy (AFM, CYPHER S, Oxford) was used to characterize the height of different nanosheets.

Electrochemical measurement

A polished 2×2 mm^2 glassy carbon (GC) electrode served as the working electrode; a Pt net electrode was used as the counter electrode; and a Hg/HgO electrode was used as the reference electrode. An electrochemical workstation (V46840, Ivium) measured the current-voltage curve in a three-electrode configuration with 1 M $[Cu(NH_3)_4]SO_4 \bullet xH_2O$ as the electrolyte.

Molecule reaction imaging

Molecule reaction images were captured using inverted fluorescence microscopy (ECLIPSE Ti2-E, Nikon) with an oil immersion objective (60×, numerical aperture of 1.49, Nikon) and a scientific complementary metal–oxide–semiconductor (sCMOS) camera (Kinetix, Teledyne Photometrics). The (photo)electrodeposition experiments were performed using an electrochemical workstation (V46840, Ivium) with a three-electrode system. The working electrode was the modified ITO decorated with nanosheets immobilized on its surface, while the reference and counter electrodes were Hg/HgO and Pt wire electrodes, respectively. The electrolyte was 1 M $[Cu(NH_3)_4]SO_4 \bullet xH_2O$. For the electrochemical deposition (ED) experiment, the processes were observed in epi mode. For the photoelectrochemical deposition (PED) experiment, the widefield laser or the focused laser was used for stimulating the material to generate carriers while the processes were monitored in

epi mode. The laser wavelength was 640 nm. The widefield laser power was 4 mW (0.25 kW cm^{-2}). The focused laser power was 0.04 mW (10 kW cm^{-2}). The exposure time was 50 ms (19.812 Hz).

The chemical deposition experiments used chloroauric acid as an oxidant and the nanosheets as a reductant agent. To obtain better contrast, the chemical reduction of HAuCl4 was observed in trans-illumination mode. The exposure time was 50 ms (19.812 Hz), and the interval time was 1 min.

Image Analysis

A “difference” operation was performed to subtract the background so that the deposition on the surface of the nanosheets can be clearly observed. The “difference” operation uses the image calculator function “difference” in ImageJ to extract the signal difference between each frame in the stack and the first frame, which can effectively remove the background.

Supplementary Figures

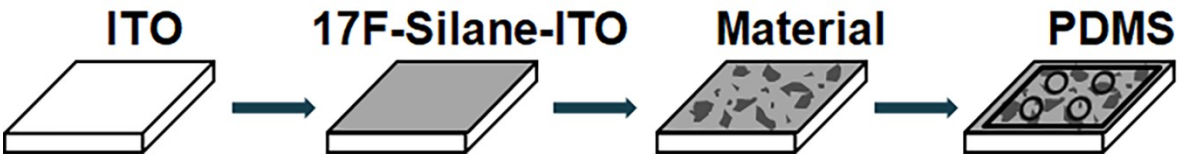

Fig. S1 Surface modification of ITO electrode.

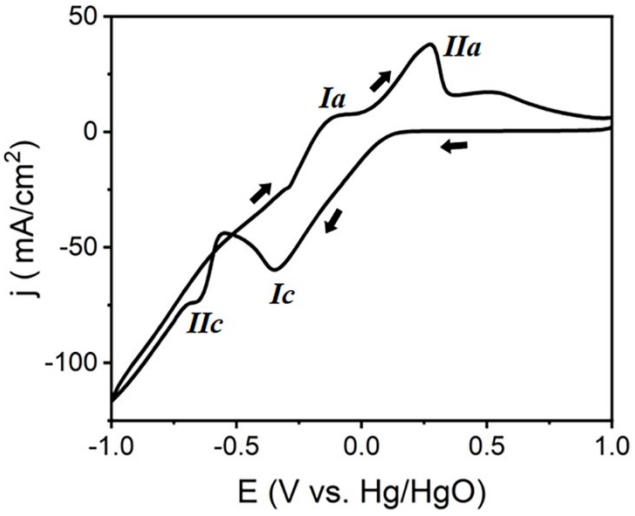

Fig. S2 CV curve of 1 M $[Cu(NH_3)_4]SO_4 \bullet xH_2O$ (pH = 9.7). The working electrode, counter electrode and reference electrode are glassy carbon electrode, platinum mesh electrode and Hg/HgO electrode, respectively. Scan rate: 20 mV/s.

At pH 9.7, the complex forms of cupric ion is soluble copper, Cu(II) predominates as $Cu(NH_3)_4^{2+}$ and Cu(I) predominates as $Cu(NH_3)_2^{+}$.[1, 2] Cyclic voltammetry is conducted within the potential range from −1.0 to 1.0 V vs Hg/HgO electrode in the negative direction (Fig. S2). The curve exhibits two cathodic peaks and two anodic peaks. The first cathodic peak, denoted as *Ic*, emerges at −0.35 V, corresponding to the reduction of $Cu(NH_3)_4^{2+}$ to $Cu(NH_3)_2^{+}$, as represented by Reaction S1. Subsequently, the second cathodic peak, labeled as *IIc*, appears at −0.66 V, indicative of the electrodeposition of copper from $Cu(NH_3)_2^{+}$ to Cu^0, as described by Reaction S2. At more negative potentials, the direct reduction of cupric ammine to metallic copper occurs when $Cu(NH_3)_2^{+}$ is depleted.

$$Cu(NH_3)_4^{2+} + e^- = Cu(NH_3)_2^{+} + 2NH_3 \quad \text{(S1)}$$

$$Cu(NH_3)_2^{+} + e^- = Cu^0 + 2NH_3 \quad \text{(S2)}$$

This voltammogram exhibits evident nucleation characteristics. In the reverse scan, two crossing potentials are observed in the cathode region. The crossover potential near the cathode peak *IIc* represents the nucleation overpotential, which corresponds to the reversible potential of metal redox couples deposited by ions in solution[3, 4]. Following this, two anodic peaks emerge. The first anodic peak, denoted as *Ia*, manifests at −0.1 V, corresponding to the oxidation of metallic copper, as described by Reaction S3. Subsequently, the generated cupric species further oxidizes metallic copper to the cuprous species, as represented by Reaction S4. Finally, the second anode peak, labeled as *IIa*, appears at 0.27 V, corresponding to the oxidation of $Cu(NH_3)_4^+$ to $Cu(NH_3)_4^{2+}$, as depicted by Reaction S5.

$$Cu^0 + 4NH_3 = Cu(NH_3)_4^{2+} + 2e^- \quad \text{(S3)}$$

$$Cu^0 + Cu(NH_3)_4^{2+} = 2Cu(NH_3)_2^+ \quad \text{(S4)}$$

$$Cu(NH_3)_2^+ + 2NH_3 = Cu(NH_3)_4^{2+} + e^- \quad \text{(S5)}$$

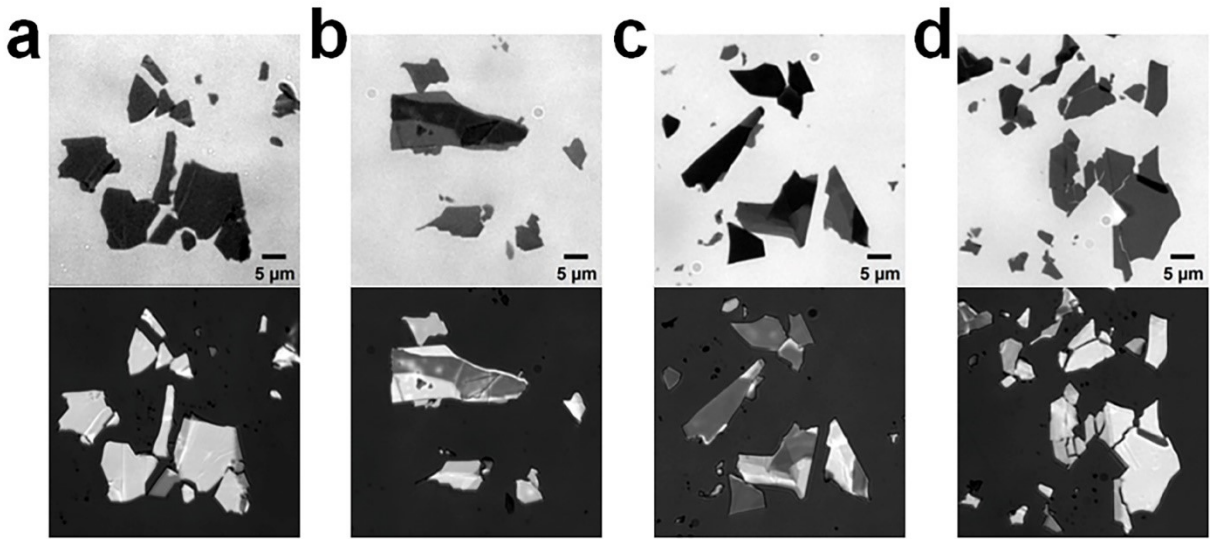

Fig. S3 Bright-field transmission images (top) and reflection images (bottom) of (a−b) n-type MoS_2 and (c−d) p-type WSe_2 nanosheets on the ITO electrodes.

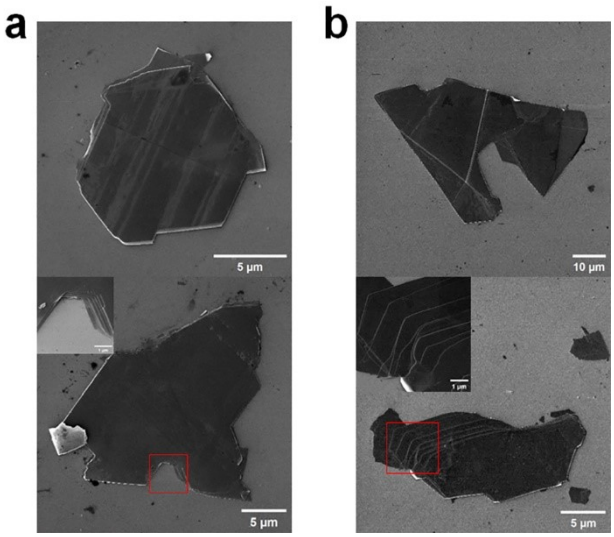

Fig. S4 Helium ion microscopy (HIM) result of (a) n-type MoS_2 and (b) p-type WSe_2 nanosheets on the ITO electrodes. Inset: enlarged HIM image of the red box.

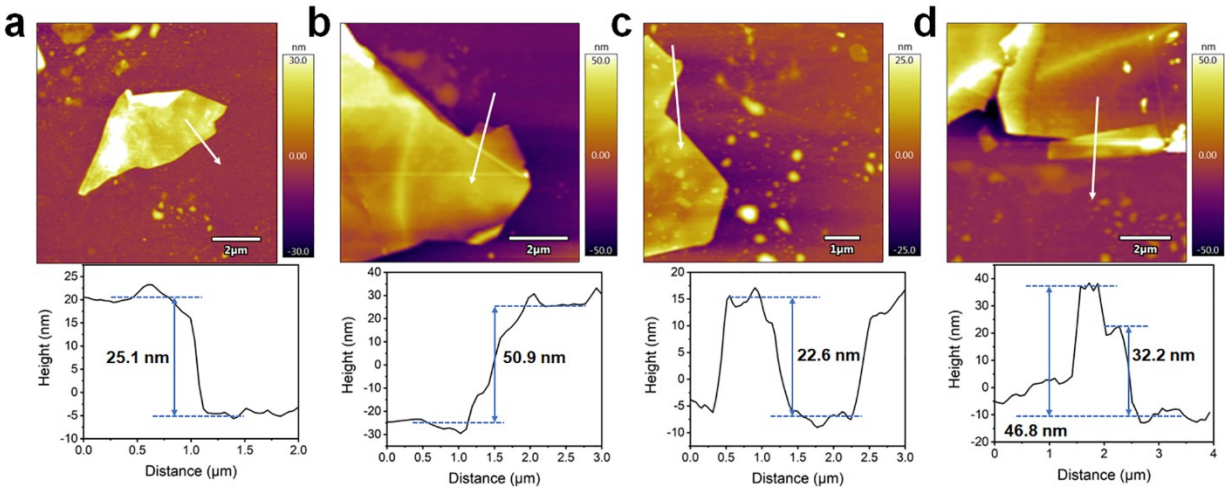

Fig. S5 Atomic force microscopy (AFM) result of (a-b) n-type MoS_2 and (c-d) p-type WSe_2 nanosheets on the ITO electrodes.

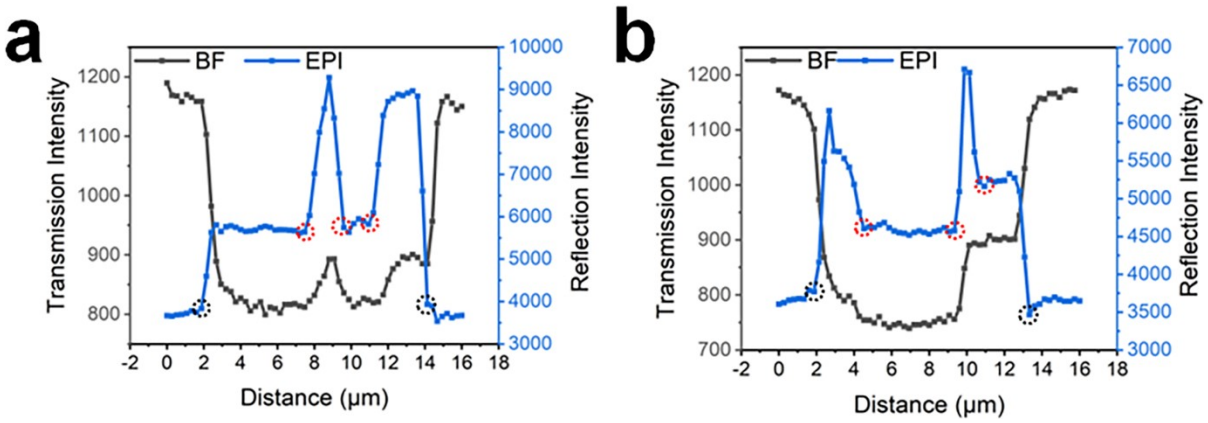

Fig. S6 Transmission intensity (black) and reflection intensity (blue) profiles of n-type MoS_2. (a, b) acquired along the white arrows in Fig. 2a and 2c, respectively. Black and red circles represent the positions of the perimeter edges and interior steps, respectively.

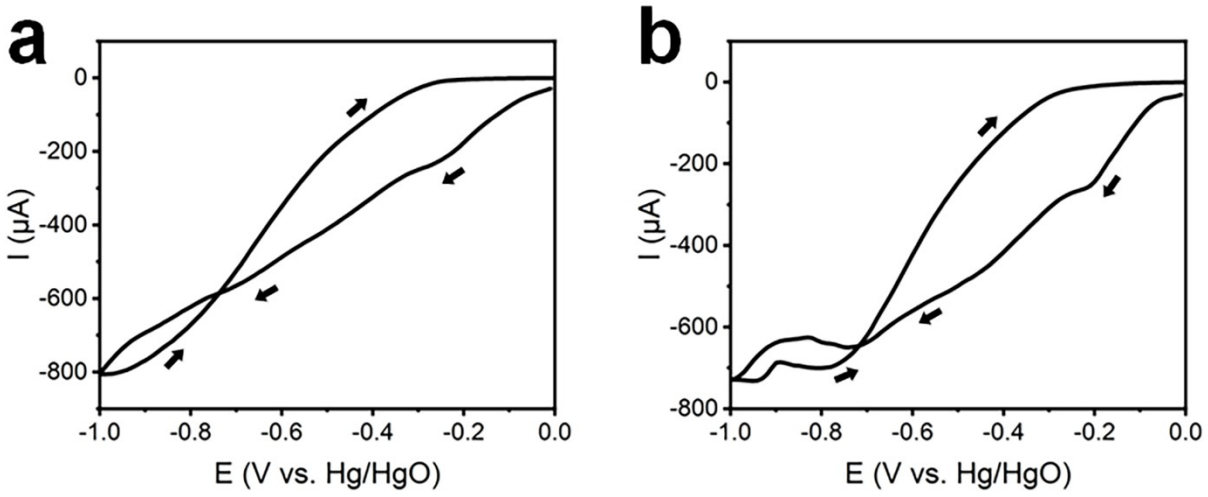

Fig. S7 CV curve of modified ITO with MoS_2 nanosheets immobilized on its surface as the working electrode in different condition. (a) Only epi-illumination. (b) Epi-illumination and 640 nm widefield laser irradiation for stimulating MoS_2 to generate carriers. The results are collected in the Cu deposition experiment, as shown in Fig. 2. The electrolyte was 1 M $[Cu(NH_3)_4]SO_4 \bullet xH_2O$ (pH = 9.7). The counter electrode and reference electrode were Pt wire electrode and Hg/HgO electrode, respectively. Scan rate: 20mV/s.

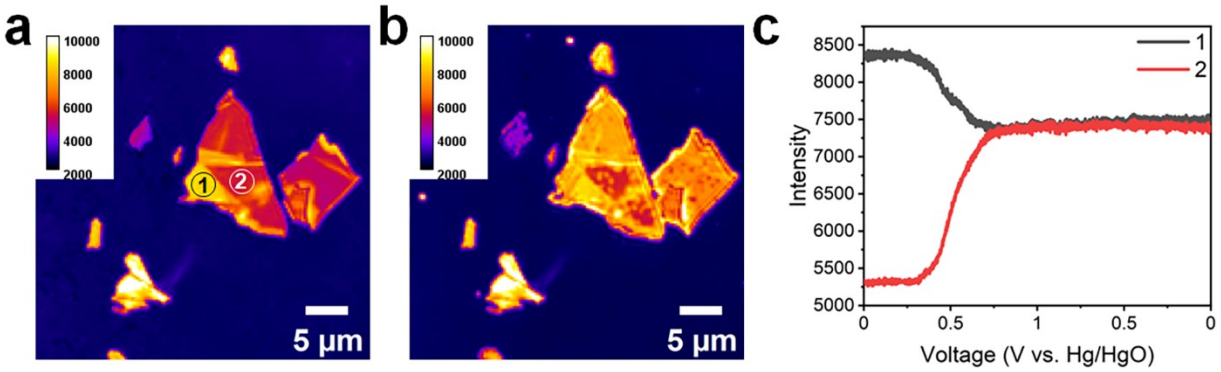

Fig. S8 Reflection image of n-type MoS_2 (a) pristine and (b) after deposition. (c) Reflection intensity *vs.* potential curve of the marked section area in (a). Area 1 represents the stronger-intensity region, and area 2 represents the lower-intensity region.

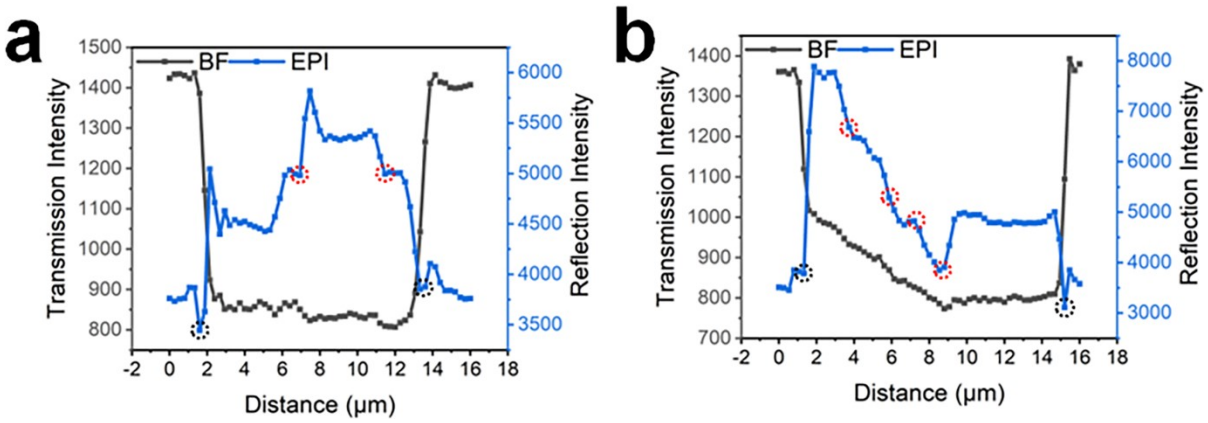

Fig. S9 Transmission intensity (black) and reflection intensity (blue) profiles of p-type WSe_2. (a, b) acquired along the white arrows in Fig. 3a and 3c, respectively. Black and red circles represent the positions of the perimeter edges and interior steps, respectively.

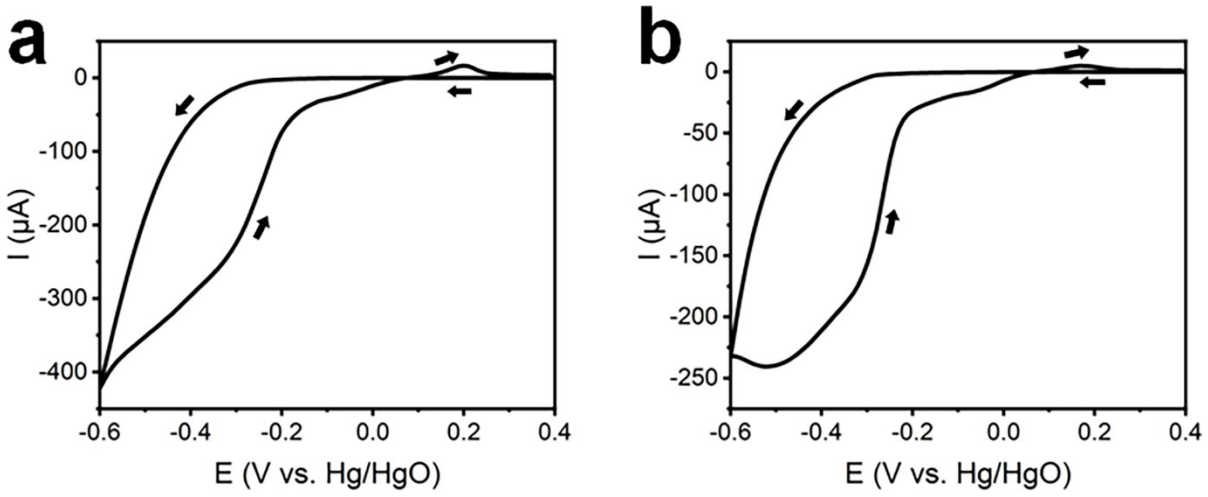

Fig. S10 CV curve of modified ITO with WSe_2 nanosheets immobilized on its surface as the working electrode under different condition. (a) Only epi-illumination. (b) Epi-illumination and widefield 640 nm laser irradiation for stimulating MoS_2 to generate carriers. The results were collected in the Cu deposition experiment, as shown in Fig. 3. The electrolyte was 1 M $[Cu(NH_3)_4]SO_4 \bullet xH_2O$ (pH = 9.7). The counter electrode and reference electrode were Pt wire electrode and Hg/HgO electrode, respectively. Scan rate: 20 mV/s.

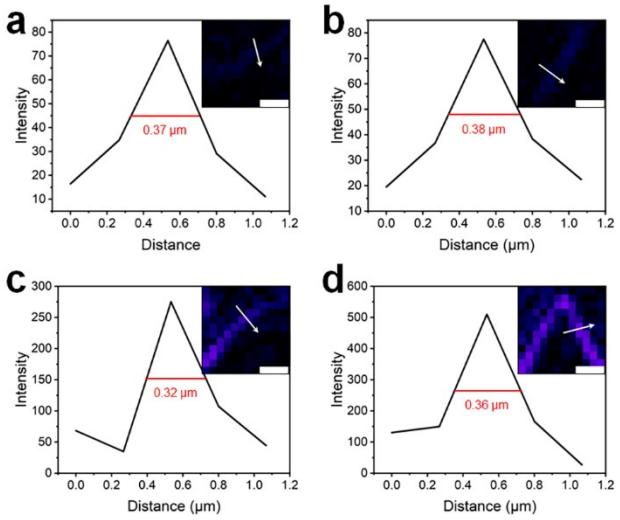

Fig. S11 Reflection intensity profiles of p-type WSe_2 nanoplates (Inset: molecular reaction imaging of deposition after "difference" operation of the p-type WSe_2; scale bar: 1 μm).

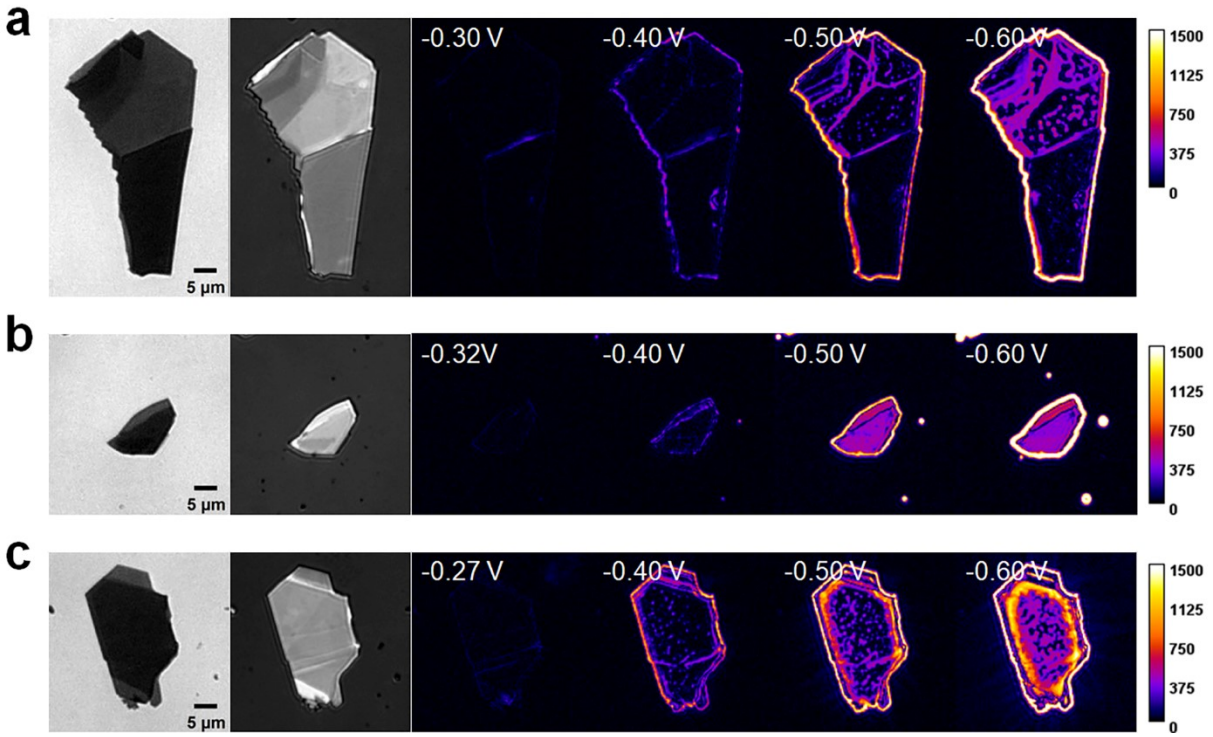

Fig. S12 Bright-field transmission images (left) and reflection images (center) of n-type MoS_2 nanosheets and molecular reaction imaging of PED (right) with different laser densities (a) 0.05 kW cm^{-2}; (b) 1.5 kW cm^{-2}; (c) 0.2 kW cm^{-2}.

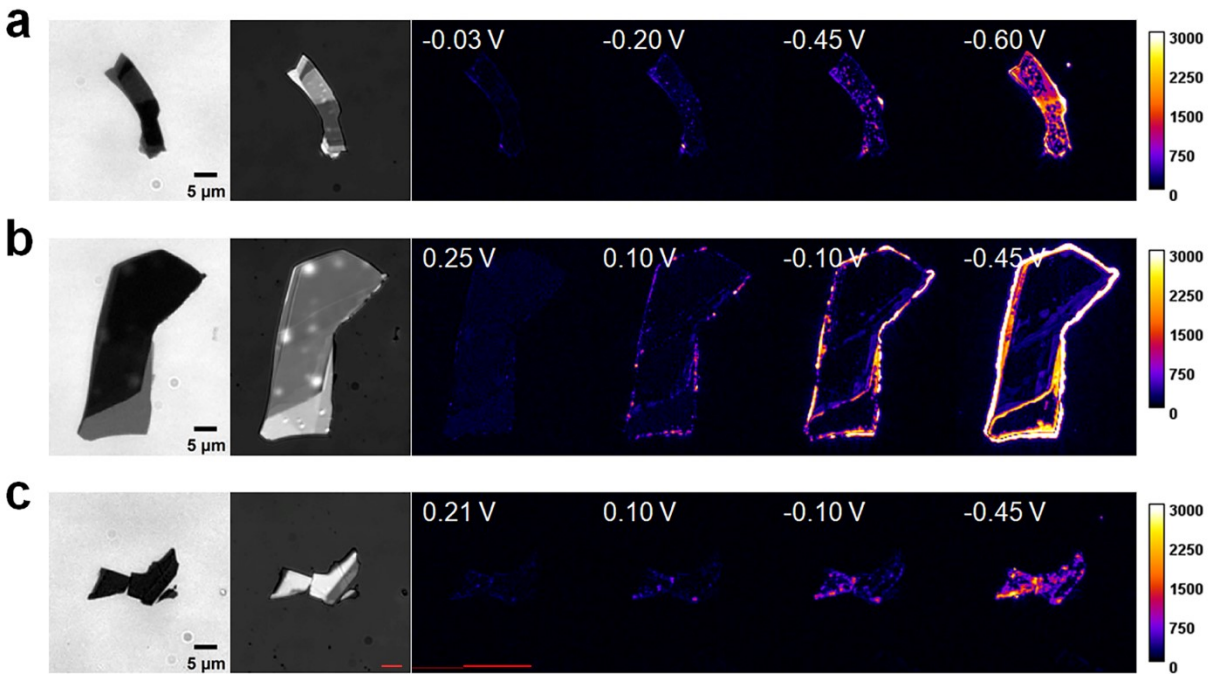

Fig. S13 Bright-field transmission images (left) and reflection images (center) of p-type WSe_2 nanosheets and molecular reaction imaging of photoelectrodeposition (right) with different laser densities (a) 0.025 kW cm^{-2}; (b) 0.1 kW cm^{-2}; (c) 0.15 kW cm^{-2}.

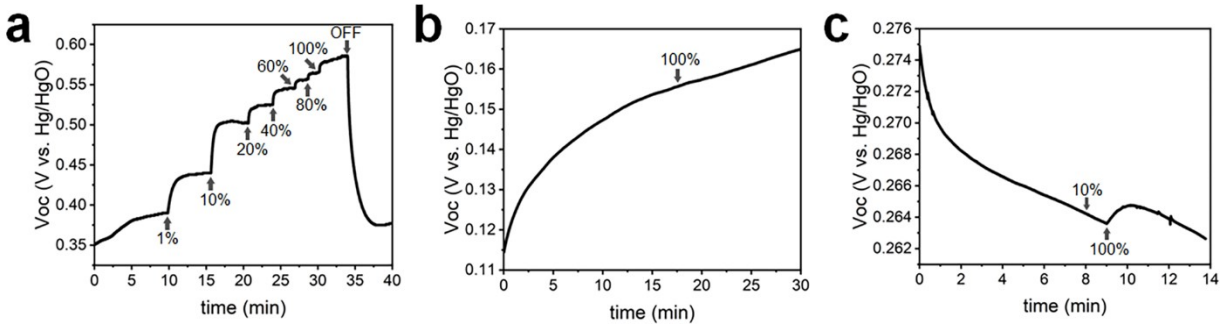

Fig. S14 Response of different substrates' open circuit voltage (V_{oc}) to laser density (100% is 0.25 kW cm^{-2}). (a) Modified ITO with WSe_2 nanosheets; (b) Modified ITO with MoS_2 nanosheets; (c) Modified ITO.

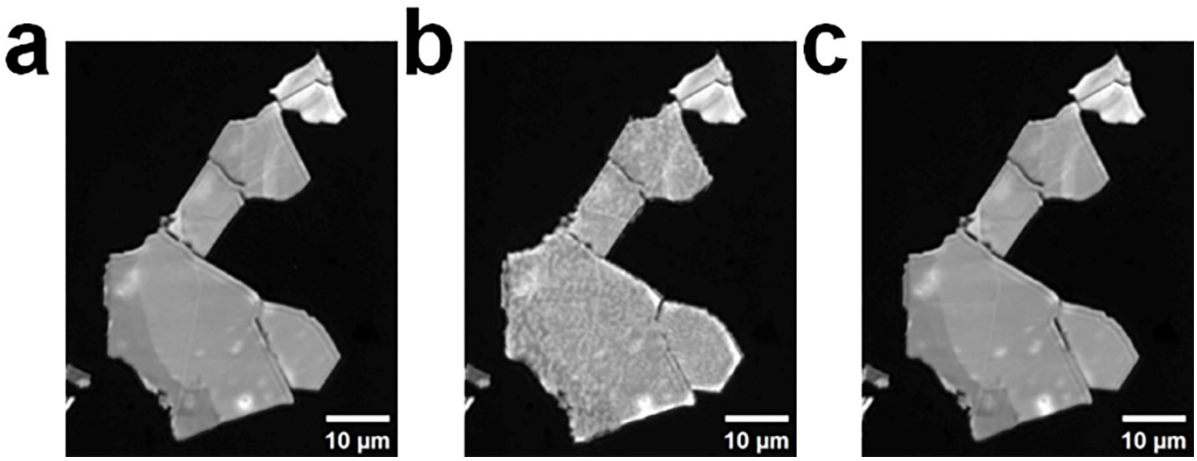

Fig. S15 (a) Reflection image of MoS_2 before ED. (b) Reflection image of MoS_2 after ED. (c) Reflection image of MoS_2 after deposited Cu is dissolved.

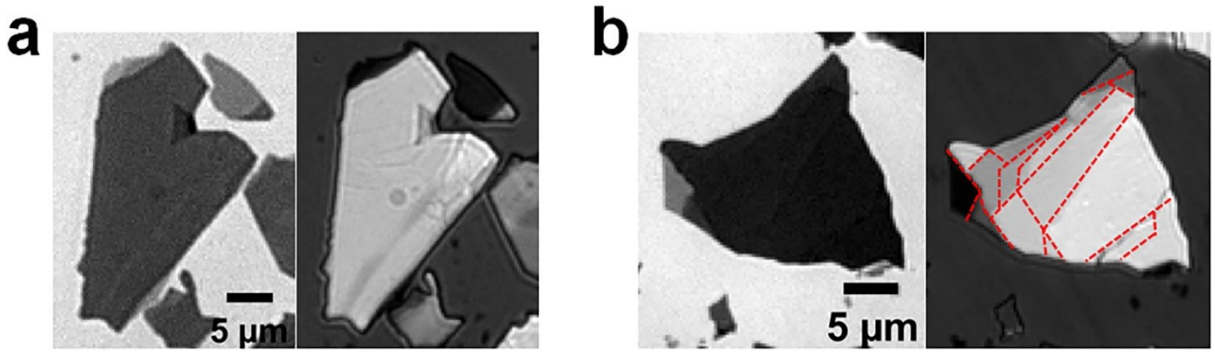

Fig. S16 (a) Bright-field transmission image (left) and reflection image (right) of n-type MoS_2 nanosheet used in Fig. 6. (b) Bright-field transmission image (left) and reflection image (right) of p-type WSe_2 nanosheets used in Fig. 7. Red dashed lines represent interior steps.

REFERENCES

1 C. Nila and I. González, The role of pH and Cu(II) concentration in the electrodeposition of Cu(II) in NH_4Cl solutions, Journal of Electroanalytical Chemistry, 1996, 401, 171-182.

2 D. Grujicic and B. Pesic, Reaction and nucleation mechanisms of copper electrodeposition from ammoniacal solutions on vitreous carbon, Electrochimica Acta, 2005, 50, 4426-4443.

3 J. Vazquez-Arenas, I. Lazaro and R. Cruz, Electrochemical study of binary and ternary copper complexes in ammonia-chloride medium, Electrochimica Acta, 2007, 52, 6106-6117.

4 F. De la Rosa and A. Ramos, Study of the Copper Electrodeposition on Titanium Electrodes, ECS Transactions, 2010, 29, 155.